Correspondence between Hanbury-Brown–Twiss radii and the emission zone in noncentral heavy ion collisions

E. Mount, G. Graef, M. Mitrovski, M. Bleicher, and M. A. Lisa

Correspondence between HBT radii and the emission zone in non-central heavy ion collisions.

E. Mount,[1] G. Graef,[2,3] M. Mitrovski,[2] M. Bleicher,[2,3] and M.A. Lisa[1]

[1]*Department of Physics, Ohio State University, Columbus, Ohio 43210, USA*
[2]*Frankfurt Institute for Advanced Studies, Frankfurt am Main, Germany*
[3]*Institut für Theoretische Physik, Goethe-Universität, Frankfurt am Main, Germany*

In non-central collisions between ultra-relativistic heavy ions, the freeze-out distribution is anisotropic, and its major longitudinal axis may be tilted away from the beam direction. The shape and orientation of this distribution are particularly interesting, as they provide a snapshot of the evolving source and reflect the space-time aspect of anisotropic flow. Experimentally, this information is extracted by measuring pion HBT radii as a function of angle with respect to the reaction plane. The connection between measured radius oscillations and the underlying geometry is neccessarily model-dependent; many existing formulae are strictly valid only for Gaussian sources with no collective flow. With a realistic transport model of the collision, which generates flow and non-Gaussian sources, we find that these formulae approximately reflect the anisotropy of the freezeout distribution.

I. INTRODUCTION

Femtoscopic intensity interferometry measurements use two-particle correlation functions to probe the space-time substructure of the system generated in heavy ion collisions, at the femtometer scale. At relativistic collision energies, extensive systematic studies have mapped out this substructure as a function of transverse momentum (p_T), rapidity (y), collision energy ($\sqrt{s_{NN}}$) and the mass of the two correlated particles; see [1] for a recent review. These measurements probe the space-time geometry of the freezeout distribution– the distribution of last-scattering points of the particles. In addition to the source size and lifetime at freezeout, the momentum-dependence of the femtoscopic scales reveal the coordinate-space aspects of collective motion– "flow."

It has long been recognized that measurements relative to the direction of the impact parameter of the collision are more sensitive to important underlying physics of the system, than are angle-integrated measurements. The azimuthal dependence of particle yields and spectra– often called "directed" and "elliptical flow"– are extensively used to extract the QCD equation of state (EoS) and transport coefficients of the quark-gluon plasma such as viscosity [2, 3]. On the other hand, azimuthally-integrated p_T spectra can flag the existence of collective behavior, but are not as discriminating between different models producing such behavior [e.g. 4, 5]. Similarly, the azimuthal dependence of jet quenching is a more discriminating probe of partonic energy loss, than azimuthally-integrated measurements [6–8].

It is possible that azimuthally-differential analysis might yield a similar improvement in sensitivity of femtoscopy. Only a few measurements of femtoscopic pion correlations relative to the impact parameter have been reported [9–11], though an extensive energy-dependence of these measurements is underway at RHIC [12].

Most experimental analyses extract so-called "HBT radii" by fitting the measured correlation function with a functional form that assumes a Gaussian emission source (c.f. discussion in [1]). In heavy ion collisions, there has been considerable activity in measuring the non-Gaussian features of the source

via "imaging" techniques [13, 14] that fit the source with a sum of spline functions. Large non-Gaussian tails are mostly explained by long-lived resonance production [15].

Gaussian HBT radii seek to capture the bulk scales of particular interest; several studies exist, testing the correspondence between HBT radii and the source scales of non-Gaussian, flowing distributions from cascade calculations [16, 17] and blast-wave and hydrodynamical models [18].

Moving beyond HBT radii themselves, which characterize the geometry only of subsets ("homogeneity regions" [19]) of the overall source, one is interested in the shape and orientation of the emission region as a whole. Here again, the connection between measured radius oscillations and the underlying anisotropic geometry is model-dependent. In the simplest case of a Gaussian source with no collective flow, all features of the anisotropic source may be extracted directly from the oscillating radii [20]. Collective flow complicates the situation considerably, since the homogeneity region probed by pions emitted in the reaction plane might be entirely disconnected from the region probed by pions emitted out of the reaction plane. Several groups have calculated HBT radius oscillations for flow-dominated blast-wave [21, 22] and hydrodynamic [23–26] models. All found that the correlation between source shapes and radius oscillations is to a greater or lesser degree complicated by the details of the collective flow in the model.

It is therefore important to quantitatively evaluate the reliability of formulae used to estimate source shapes from experimental HBT radii. Retiere and Lisa have propsed [21] an expression connecting the azimuthal oscillations of HBT radii with the transverse anisotropic shape of the source. This expression is strictly correct only for Gaussian, non-flowing sources; however, even for flow-dominated boost-invariant hydrodynamic simulations and for realistic blast-wave scenarios, the expression reliably reproduced the source anisotropy to within 30%. In this paper, we test this expression in the context of a realistic transport model featuring non-Gaussian freezeout distributions and strong flow. We also present and test an additional formula– again strictly valid only for Gaussian, non-flowing systems– to estimate the tilt of the source

relative to the beam direction. We find reasonable consistency between the source eccentricity and tilt as extracted directly from the space-time freezeout coordinates, and the same quantities estimated with the formulae. The discrepancy between the two provides an estimate of the systematic uncertainty one expects, when using azimuthally-differential pion correlation measurements to extract the underlying source shape and orientation.

In section II, we define the formalism and the connection between HBT radii and an anisotropic but simplified static Gaussian source. There, we present formulae connecting measurable quantities to the interesting features of the geometry. In section III, a realistic transport model (UrQMD) is used to generate a freezeout distribution featuring non-Gaussian geometry and strong collective flow. We discuss the non-trivial anisotropies of the distribution and the relationship between regions of homogeneity [19, 27] and the "whole" source of emission points. In section IV, we simulate an experimental analysis, using the UrQMD-generated distributions. We build two-pion correlation functions and use the formulae presented in section II to estimate the source anisotropies. The calculations are compared to reported experimental results from Au+Au collisions at $\sqrt{s_{NN}} = 3.84$ GeV, and predictions are given for heavy ion collisions at $\sqrt{s_{NN}} = 30$ GeV, relevant for FAIR and the RHIC energy scan. In section V, we summarize.

II. HBT RADII AND THEIR CONNECTION TO THE UNDERLYING SOURCE

Femtoscopic two-particle correlation functions as a function of the relative momentum $q = p_1 - p_2$ are often fitted in terms of Gaussian HBT radii $R_{i,j}^2$

$$C(q) = 1 + \lambda \exp\left(-\sum_{i,j=o,s,l} q_i q_j R_{i,j}^2\right). \quad (1)$$

Indices i and j indicate the components of the q vector in the so-called Bertsch-Pratt "out-side-long" coordinate system [28–30]. Here, "out" points along the direction of the pair transverse momentum, and "long" points along the direction of motion of one of the incoming nuclei, say, in the direction of Au ions in the yellow ring of RHIC. We shall call this the "yellow nucleus" and its colliding partner the "blue nucleus." (We return to this arbitrary designation soon.) The "side" direction is given by the cross-product of "out" with "long." It is worthwhile to point out that, while one may simultaneously flip the signs of all components of q by swapping the designation of particles 1 and 2, the correlation function depends only on even-order products of q's components; these products have meaningful sign.

We begin by considering a simple source of midrapidity pions which is a Gaussian ellipsoid in space and time, with the major axis of the ellipse tilted with respect to the beam direction, as sketched in Figure 1. The distribution is characterized by five parameters: a temporal scale, three spatial scales and
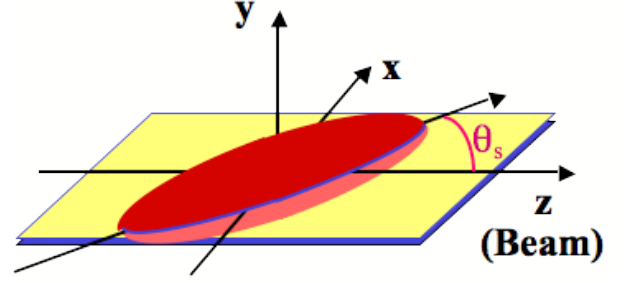

FIG. 1: (color online) The simplified parameterization of the freeze-out distribution in a heavy ion collision. In addition to the timescale and three spatial length scales, the ellipsoid may be tilted in the direction of the impact parameter x, relative to the beam axis z.

a tilt angle

$$f(x,y,z) \sim \exp\left(-\frac{(x\cos\theta_s - z\sin\theta_s)^2}{2\sigma_{x'}^2} - \frac{y^2}{2\sigma_y^2} - \frac{(x\sin\theta_s + z\cos\theta_s)^2}{2\sigma_{z'}^2} - \frac{t^2}{2\sigma_t^2}\right), \quad (2)$$

where the primes on $\sigma_{x'}$ and $\sigma_{z'}$ signify that these correspond to principle axes of the ellipse.

Its transverse eccentricity about its (tilted) major axis is defined as

$$\varepsilon' \equiv \frac{\sigma_y^2 - \sigma_{x'}^2}{\sigma_y^2 + \sigma_{x'}^2} \quad (3)$$

If $\theta_s = 0$ and $\sigma_x = \sigma_y \equiv \sigma_\perp$ (or equivalently in an azimuthally-integrated analysis), only three parameters characterize the source, and the HBT radii are given by

$$\begin{aligned} R_s^2 &= \sigma_\perp^2 \\ R_o^2 &= \sigma_\perp^2 + \beta_\perp^2 \sigma_t^2 \\ R_l^2 &= \sigma_z^2 + \beta_l^2 \sigma_t^2, \end{aligned} \quad (4)$$

where $\beta_\perp$ and β_l are the transverse and longitudinal velocities of the pion pair. "Cross-term" radii $R_{i\neq j}^2$ vanish by symmetry [20, 31].

For the more general case, there are six HBT radii, and they depend on the azimuthal angle ϕ. This angle is meaningfully defined over the range $[0,2\pi]$ about the beam direction relative the impact parameter, which is defined as the direction perpendicular to the beam, pointing *from* the yellow nucleus *to* the blue one. Swapping the designations of the "yellow" and "blue" nuclei reverses the direction of the impact parameter (x direction); however, it also reverses the "long" (z) direction, defined earlier. Hence, the sense of the tilt θ_S is well-defined; a source with positive tilt features a positive spatial $x - z$ correlation, as shown in figure 1. Experimental measurement of the sense of the tilt [9] requires measuring the direction of the impact parameter, for example through directed flow of net baryons at forward rapidity.

The HBT radii, measured as a function of angle ϕ relative to the beam axis, are driven by source widths $\sigma_x, \sigma_y, \sigma_z$, rather than $\sigma_{x'}, \sigma_y, \sigma_{z'}$. The relationships between these widths are given by

$$\sigma_{x'}^2 = \sigma_x^2 \cos^2\theta_s + \sigma_z^2 \sin^2\theta_s + \sigma_{xz}^2 \sin 2\theta_s$$
$$\sigma_{z'}^2 = \sigma_x^2 \sin^2\theta_s + \sigma_z^2 \cos^2\theta_s - \sigma_{xz}^2 \sin 2\theta_s \quad (5)$$

where σ_{xz}^2 is the covariance between x and z in the source function; see [20] for details.

The HBT radii are related to these widths as [20]

$$R_s^2(\phi) = \tfrac{1}{2}\left(\sigma_x^2 + \sigma_y^2\right) + \tfrac{1}{2}\left(\sigma_y^2 - \sigma_x^2\right)\cos 2\phi,$$
$$R_o^2(\phi) = \tfrac{1}{2}\left(\sigma_x^2 + \sigma_y^2\right) - \tfrac{1}{2}\left(\sigma_y^2 - \sigma_x^2\right)\cos 2\phi + \beta_\perp^2 \sigma_t^2,$$
$$R_{os}^2(\phi) = \tfrac{1}{2}\left(\sigma_y^2 - \sigma_x^2\right)\sin 2\phi$$
$$R_l^2(\phi) = \sigma_z^2 + \beta_l^2 \sigma_t^2,$$
$$R_{ol}^2(\phi) = \sigma_{xz}^2 \cos\phi,$$
$$R_{sl}^2(\phi) = -\sigma_{xz}^2 \sin\phi. \quad (6)$$

In analogy with Equation 3, we identify the eccentricity of the source around the *beam* axis as

$$\varepsilon \equiv \frac{\sigma_y^2 - \sigma_x^2}{\sigma_y^2 + \sigma_x^2} \quad (7)$$

Equations 6 express the explicit ϕ-dependence of the HBT radii for a non-flowing source; all other variables in the equations are constants, for a non-flowing source. For a source with flow, the constants, e.g. σ_y, may themselves depend on ϕ. In this case, our equations will be violated; below, we quantify this violation and its effect on the extraction of θ_s and ε.

Experimentally, one measures the squared HBT radii and calculates the Fourier coefficients quantifying their azimuthal dependence, per [21, 31]

$$R_s^2(\phi) = R_{s,0}^2 + 2\sum_{n=2,4,6,\dots}R_{s,n}^2 \cos(n\phi),$$
$$R_o^2(\phi) = R_{o,0}^2 + 2\sum_{n=2,4,6,\dots}R_{o,n}^2 \cos(n\phi),$$
$$R_{os}^2(\phi) = 2\sum_{n=2,4,6,\dots}R_{os,n}^2 \sin(n\phi),$$
$$R_l^2(\phi) = R_{l,0}^2 + 2\sum_{n=2,4,6,\dots}R_{l,n}^2 \cos(n\phi),$$
$$R_{ol}^2(\phi) = 2\sum_{n=1,3,5,\dots}R_{ol,n}^2 \cos\phi$$
$$R_{sl}^2(\phi) = 2\sum_{n=1,3,5,\dots}R_{sl,n}^2 \sin\phi. \quad (8)$$

Equivalently,

$$R_{\mu,n}^2(p_T) = \begin{cases} \langle R_\mu^2(p_T,\phi_p)\cos(n\phi_p)\rangle & (\mu=o,s,l,ol) \\ \langle R_\mu^2(p_T,\phi_p)\sin(n\phi_p)\rangle & (\mu=os,sl) \end{cases}. \quad (9)$$

In our no-flow Gaussian model, then, the source geometry and orientation are extracted from the Fourier coefficents. Identifying the tilt angle requires [20, 31] measuring HBT relative to the first-order reaction plane [3]. Published results from the STAR [10] and CERES [11] collaborations use only the 2nd-order plane and so report the source eccentricity only about the beam axis. (Efforts to perform the analysis relative

to the first-order plane are underway at RHIC [12].) In this case [21]

$$\varepsilon = 2\cdot\frac{\tilde{R}_{s,2}^2}{R_{s,0}^2}. \quad (10)$$

For the moment, we ignore the tildes above the $n \neq 1$ Fourier coefficients here and below. They represent a trivial finite-binning correction discussed later in section IV.

If the first-order plane is identified, first-order azimuthal oscillations in R_{sl}^2 and R_{ol}^2 are measureable. In this case one obtains the tilt angle according to [20]

$$\theta_s = \tfrac{1}{2}\tan^{-1}\left(\frac{-4\tilde{R}_{sl,1}^2}{R_{l,0}^2 - R_{s,0}^2 + 2\tilde{R}_{s,2}^2}\right). \quad (11)$$

The transverse eccentricity in the "natural" frame tilted relative to the beam axis is

$$\varepsilon' = \frac{2\tilde{R}_{s,2}^2\left(1+\cos^2\theta_s\right) + \left(R_{s,0}^2 - R_{l,0}^2\right)\sin^2\theta_s - 2\tilde{R}_{sl,1}^2\sin 2\theta_s}{R_{s,0}^2\left(1+\cos^2\theta_s\right) + \left(2\tilde{R}_{s,2}^2 + R_{l,0}^2\right)\sin^2\theta_s + 2\tilde{R}_{sl,1}^2\sin 2\theta_s} \quad (12)$$

III. FREEZEOUT DISTRIBUTIONS FROM A MORE REALISTIC MODEL

Our simple model of the emission function given in equation 2 is unrealistic in at least two ways. Firstly, while realistic emission functions are often roughly Gaussian, they are never perfectly so; in this case, the two-pion correlation function is likewise non-Gaussian. Extracting Gaussian HBT errors through fits with equation 1, then, could in principle generate considerable mis-representation of the emission function.

The second over-simplification of the source discussed above is its lack of collective flow, which generates correlations between a particle's emission position and its momentum [19]. For example, an explosively flowing source will boost particles emitted from its right side, towards the right. The freezeout distribution of particles with a given momentum vector is known as the region of homogeneity for that momentum vector. In *principle*, the homogeity regions for different azimuthal angles might be completely disjoint and unrelated, obviously invalidating equations 6, 10, 11 and 12. In practice, the homogeneity regions in blast-wave models [21] or hydodynamic simulations [23] are naturally related. For boost-invariant sources, equation 10 is estimated to be good to $\sim 30\%$ in these models [21].

While blast-wave and boost-invariant hydro models do feature non-Gaussian sources and collective flow, they are still simplistic. Firstly, any boost-invariant model by definition has no tilt relative to the beam axis; thus they are unable to access physics associated with θ_s. Secondly, they typically use the Cooper-Frye formula to model particle freezeout from a calculated or parameterized hypersurface; while momentum-space observables (e.g. v_2) may be insensitive to this procedure, interferometry is known to be quite sensitive to the freezeout procedure.

In this section, we use the Ultra-Relativistic Quantum Molecular Dynamics Model (UrQMD 3.3)[1] to generate a realistic freeze-out distribution with fully three-dimensional dynamics [32, 33]. UrQMD is a covariant transport approach to simulate the interactions between hadrons and nuclei up to relativistic energies. It is based on the propagation of nucleons and mesons accompanied by string degrees of freedom with interaction probabilities according to measured and calculated cross sections for the elementary reactions. Hard scatterings with large momentum transfer are treated via PYTHIA. For detailed comparisons of this version to experimental data, the reader is referred to [34]. Previous HBT studies with UrQMD have been reported in [35–38].

In UrQMD, the freeze-out space-time point is naturally defined as the last hard interaction of a particle. The freezeout distribution of pions from $\sqrt{s_{NN}} = 3.84$ GeV Au+Au collisions with impact parameter $b = 4 - 8$ fm in the reaction plane ($x - z$ plane) is shown in figure 3. The source has an obvious tilt structure relative to the beam axis. We use the parameterization of equation 2 to fit the three-dimensional freezeout distribution for *all* pions with $p_T < 400$ MeV/c and $|y| < 0.6$– not only those at a given angle ϕ. From this direct analysis of the freezeout coordinates– obviously not possible in experiment– we find the parameters listed in the third column of table I. It is clear from figure 3 that $x - z$ correlation in the freezeout distribution has structure that cannot be captured in a single tilt number; indeed, the tilt is scale-dependent, growing as one focuses on the peak of the distribution. This "twist" feature, which has been observed in simulations before [20], might be physically interesting and experimentally accessible; we leave exploration of this effect for a future work. For the purpose of this work, we identify a range of tilts arising from fitting equation 2 to the distribution and varying the fit range in coordinate space from 10 fm $< \Delta x, \Delta y, \Delta z < 40$ fm. This leads to the range shown in the left column of table I.

Dynamics naturally leads to a strong correlation between a particle's final momentum and the freezeout position; homogeneity regions are naturally reflected in the final state. Figure 2 shows homogeneity regions from UrQMD in the $x - y$ plane for particles emitted at three azimtuthal angles. The homogeneity region for particles emitted at a given angle ϕ_1 clearly differs from that for particles emitted at $\phi_2 \neq \phi_1$. Thus, in addition to the *explicit* ϕ-dependence of the HBT radii seen in equations 6, there is an additional *implicit* dependence [39–42]. HBT radii measured at a given momentum vector (ϕ, p_T, y) probe only the geometry of the homogeneity region for that momentum vector. *A priori*, it is far from clear that equations 10, 11 and 12, which attempt to relate HBT radius oscillations to the geometry of the "whole" source, will prove good approximations.

In the next section, we test these relations– true for the simplest toy model of Equation 2– with UrQMD-generated freezeout distributions.
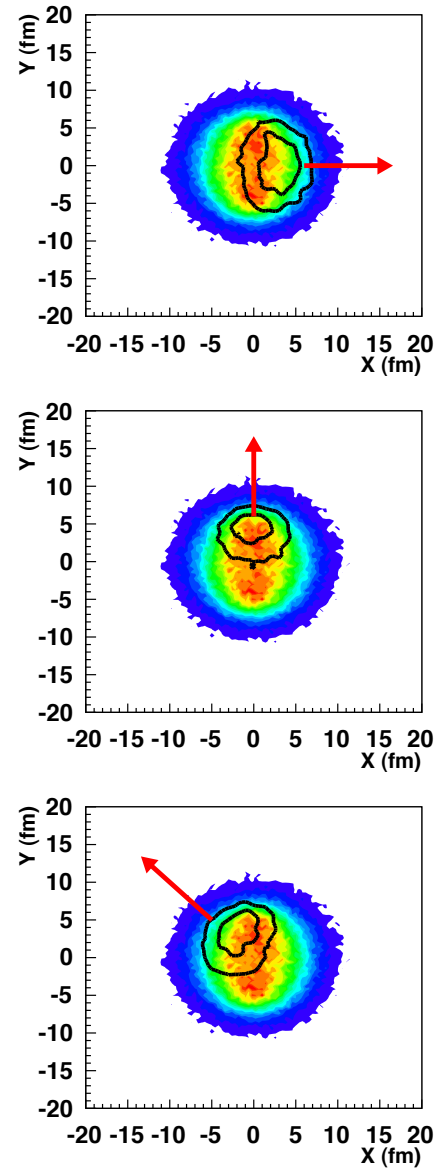

FIG. 2: (color online) Pion emission points from UrQMD simulations of Au+Au collisions with collision energy $\sqrt{s_{NN}} = 3.84$ GeV (corresponding to a 6 AGeV beam incident on a fixed target) and impact parameter $b = 4 - 8$ fm. Colored contours (identical for the three panels) show the emission point density of all pions with $p_T < 0.4$ GeV/c. Black contours in the upper, middle and lower panels indicate the density of emission points for pions with $\phi = \left[-\frac{\pi}{8}, \frac{\pi}{8}\right]$, $\left[\frac{3\pi}{8}, \frac{5\pi}{8}\right]$ and $\left[\frac{5\pi}{8}, \frac{7\pi}{8}\right]$, respectively.

IV. HBT RADII AND ANISOTROPY PARAMETERS FROM URQMD-GENERATED CORRELATION FUNCTIONS

We start by generating two-pion correlation functions, analogous to those measured experimentally, from UrQMD events. We will then proceed to fit these correlation functions with the Gaussian anzatz of equation 1, as is done in experimental analysis. Finally, we extract Fourier co-

---

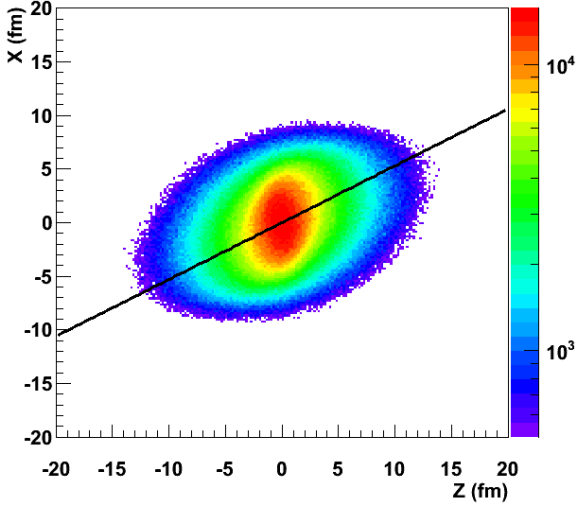[1] This version can be downloaded from www.urqmd.org.

FIG. 3: Freezeout distribution of pions from $\sqrt{s_{NN}} = 3.84$ GeV (6 AGeV beam energy on fixed target) Au+Au collisions with impact parameter $b = 4 - 8$ fm in the reaction $(x - z)$ plane, as calculated from UrQMD.

efficients characterizing the oscillations of the HBT radii with angle; from these we extract the source anisotropy parameters that would be obtained in an experiment.

To simulate experimental conditions, two-pion correlation functions were constructed from the UrQMD events using the so-called weighting method [2]. In this method, pairs of identical pions are selected according to a Monte Carlo algorithm; the correlation function in a given (q_o, q_s, q_l) bin is equal to the pair-wise average of the squared two-pion squared wavefunction. Considering only quantum symmetrization effects, the correlation function is computed as

$$C(q_o, q_s, q_l; \phi) = \langle 1 + \cos(-q^\mu \Delta r_\mu) \rangle_\phi, \qquad (13)$$

where $q = p_1 - p_2$ is the relative momentum and Δr is the space-time separation of the particles at freezeout.

As explicitly denoted in equation 13, the correlation functions were generated for 8 $45°$-wide bins in pair angle $\phi \equiv \angle(\vec{K}_T, \vec{b})$, where $\vec{K}_T \equiv (\vec{p}_{T,1} + \vec{p}_{T,2})/2$ is the average transverse momentum vector of the pair. Hence, for $-\frac{\pi}{8} < \phi < \frac{\pi}{8}$ ($\frac{5\pi}{8} < \phi < \frac{7\pi}{8}$), pions from sub-region indicated by the black contours in the top (bottom) panel of figure 2 are used to construct the correlation function.

In figure 4 are plotted, for each bin in ϕ, two-dimensional slices of the three-dimensional correlation function in the $q_o - q_s$, $q_s - q_l$ and $q_l - q_o$ planes; in each case the unplotted relative momentum component $q_i < 4$ MeV/c. For a representative ϕ bin, one-dimensional slices of the correlation function in the out, side, and long directions are shown in Figure 5. Most femtoscopic correlation analyses focus on the
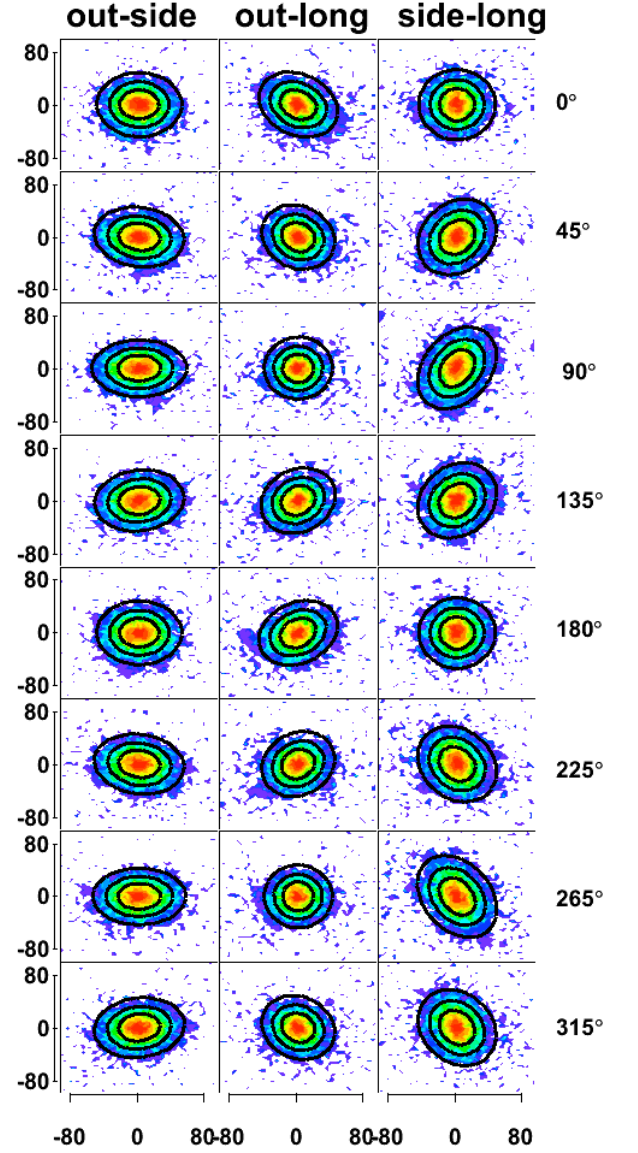
FIG. 4: (color online) Pion correlation functions from Au+Au collisions with collision energy $\sqrt{s_{NN}} = 3.84$ GeV and (corresponding to a 6 AGeV beam incident on a fixed target) and impact parameter $b = 4 - 8$ fm, as calculated with the UrQMD model. Projections in the $q_o - q_s$ (left column), $q_o - q_l$ (middle) and $q_s - q_l$ spaces are made, with the unplotted $\vec{q}$-component smaller than 4 MeV/c. Correlation slices are shown for pion pairs in $45°$-wide ϕ bins centered at angles indicated to the right of each row. Shaded (color online) contours represent the calculated correlation function. Black contours represent 2-dimensional slices of the three-dimensional Gaussian fit to the correlation functions for each selection in ϕ.

one-dimensional projections, since the correlation in three-dimensional space factorizes; that is, there is no covariance between components q_i and $q_{j \neq i}$ in the correlation function. This is not the case when the analysis is performed differentially in ϕ [9, 20, 31, 39–42], as is clear from the tilted structures in $\vec{q}$-space seen in figure 4. These tilts in the individual correlation functions in $\vec{q}$-space for a given angular selction
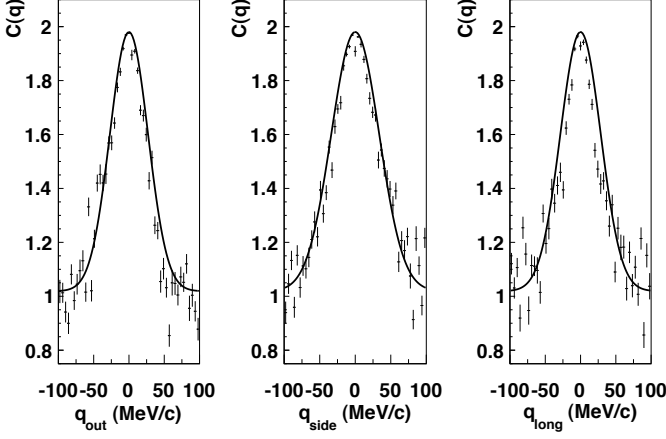
FIG. 5: One dimensional slices in the three components of relative momentum, for pions emitted at $|\phi| < 22.5°$. Curves represent one-dimensional slices of the three-dimensional Gaussian fit to the correlation function.

FIG. 6: The six HBT radii extracted from Gaussian fits (equation 1) to the correlation functions for eight selections on ϕ. Curves represent a Fourier decomposition (equation 9), including terms up to second order, where the Fourier components are determed according to equation 9. See text for details.

FIG. 7: Same as figure 6, but for collisions at $\sqrt{s_{NN}} = 7.7$ GeV.

in $\vec{K}$ are not to be confused with the overall spatial tilt of the source sketched in figure 1.

As in an experimental analysis, the correlation functions are fitted with the Gaussian functional form of equation 1. Two- and one-dimensional slices of these fits are superimposed on the correlation functions in figures 4 and 5. The six resulting HBT radii are plotted as a function of ϕ on figure 6. As in a standard azimuthally-integraged analysis, the "diagonal" radii R_j^2, $j = o, s, l$ are driven by the width of the correlation function in the direction j. The "cross-term" radii $R_{i, j \neq i}^2$ quantify the correlations between $\vec{q}$ components– the tilts of the correlation function; e.g. the ϕ-dependence of the tilt of the correlation function in the $q_s - q_l$ space seen in the right column of figure 4 leads directly to the first-order oscillation of R_{sl}^2 seen in figure 6. Figure 7 shows the radii for $\sqrt{s_{NN}} = 7.7$ GeV collisions.

The curves on figures 6 and 7 represent equations 9 using Fourier coefficients $R_{\mu,n}^2$ calculated according to 9.

Before we apply equations 10-12, we note that the argumentation of section II implicitly assumed that the $R_\mu^2(\phi)$ were measured as a continuous function. In reality, in our analysis as in experiment, the correlation function is measured for ϕ within bins of width $\Delta\phi$. The amplitude of the nth-order oscillation of a binned function is reduced from that of the underlying function. To correct for this finite-binning artifact, we calculate the underlying ("true") Fourier coefficients $\tilde{R}_{\mu,n}^2$ from the ones extracted from the binned radii by

$$\tilde{R}_{\mu,n}^2 = \frac{n\Delta\phi/2}{\sin(n\Delta\phi/2)} R_{\mu,n}^2. \qquad (14)$$

For our $45°$-wide bins, $\tilde{R}_{\mu,1}^2 = 1.026 R_{\mu,1}^2$ and $\tilde{R}_{\mu,2}^2 = 1.111 R_{\mu,2}^2$. These binning-corrected Fourier coefficients are used in equa-
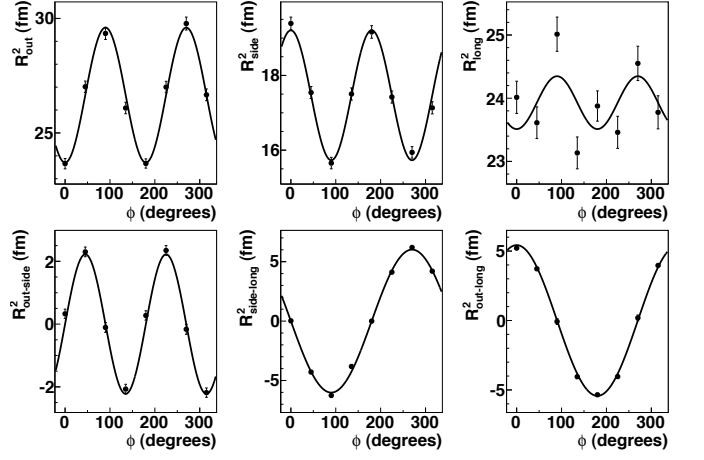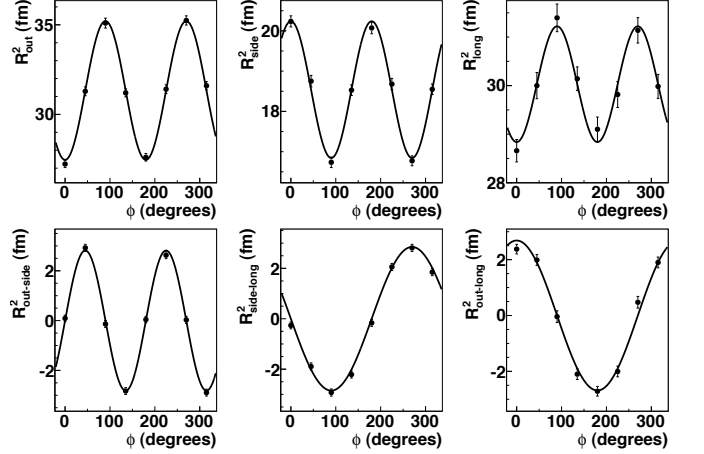
tions 10-12. [3]

As in most experimental analyses, the correlation functions from UrQMD simulations are not purely Gaussian, since the source itself is not Gaussian in coordinate space, due to space-momentum correlations (flow), resonance contributions, etc. Of special interest for the present study is the additional fact that the source is not characterized by a tilt angle independent of spatial scale– the "twist" discussed in section III. Following a standard experimental approach [e.g. 43], we perform a

_____

[3] In principle, one could correct the correlation functions themselves for the finite ϕ-binning, and then extract HBT radii from them, as described in [31]. However, especially if the reaction-plane estimation resolution [3] is good (in our model analysis, it is perfect), it makes no significant difference whether the correlation functions or the radii themselves are corrected for binning effects [49].

$\sqrt{s_{NN}}$		Direct fit to coordinate space	UrQMD: HBT oscillations	Expt.: HBT oscillations
3.84 GeV (6 AGeV)	ε	$0.13 - 0.17$	$0.095 - 0.096$	0.30 ± 0.15
	θ_s	$34° - 41°$	$27.4° - 27.9°$	$26° \pm 7°$
	ε'	$0.21 - 0.26$	$0.200 - 0.206$	0.38 ± 0.19
7.7 GeV (30 AGeV)	ε	$0.11 - 0.14$	$0.090 - 0.091$	-
	θ_s	$14° - 21°$	$11.7° - 11.9°$	-
	ε'	$0.12 - 0.16$	0.109	-

TABLE I: Source anisotropy parameters, for Au+Au collisions at two collision energies, with $b = 4 - 8$ fm for pions with $p_T < 0.6$ GeV/c, and $|y| < 0.6$. Impact parameter and momentum cuts were selected to match published data from the E895 collaboration [9]. Third column: estimates from a Gaussian fit (equation 2) to the freezeout distribution from UrQMD events. Fourth column: estimates using equations 10-12 on the azimuthal oscillations of HBT radii from UrQMD events. Fifth column: same as column four, but using experimental data from E895. Experimental data at 7.7 GeV will be analyzed at FAIR and RHIC.

fit-range study, in which we vary the range in q_o, q_s, q_l, over which we perform the fit with equation 1. In particular, we fit the correlation functions in the range $-q_{max} < q_o, q_s, q_l < q_{max}$ for $q_{max} = 60 - 150$ MeV/c. The resulting anisotropy parameters for $\sqrt{s_{NN}} = 3.84$ GeV collisions, calculated according to equations 10-12, are shown on figure 8. The dependence of θ_S on q_{max} is readily understood. Large values of q probe smaller values of coordinate space; thus, as q_{max} is increased, the fit is increasingly sensitive to the large tilt structure seen at small scales in figure 3. Figure 8, then, is itself a measure of the "twist" structure in coordinate space, though there may be more sophisticated ones. For our purposes, however, we take the variation of the anisotropy parameters plotted in figure 8 to define a range of values one might expect from an experimental study. Since a typical experimental analysis would fit at least out to 100 MeV/c (in order to include all of the peak signal), the value ranges listed in the fourth column of table I correspond to 100 MeV/c $< q_{max} < 150$ MeV/c.

The agreement with the parameters extracted via direct analysis of the UrQMD freezeout coordinates is fair; and we discuss this further in the next section.

The fifth column in table I lists the anisotropy parameters based on HBT radii measured by the E895 collaboration in a fixed-target experiment at $E_{beam} = 6$ AGeV [9]. The UrQMD calculation reproduces the tilt angle very well, the eccentricities somewhat less well, though experimental uncertainties are large. UrQMD calculations in the bottom row of the table represent a prediction for collisions at $\sqrt{s_{NN}} = 7.7$ GeV, which will be measured at FAIR and RHIC.

V. DISCUSSION AND SUMMARY

The connection between anisotropic particle emission distributions and femtoscopic correlation functions has been discussed in detail. Gaussian fits to three-dimensional two-pion correlation functions result in six HBT radii (in contrast to the
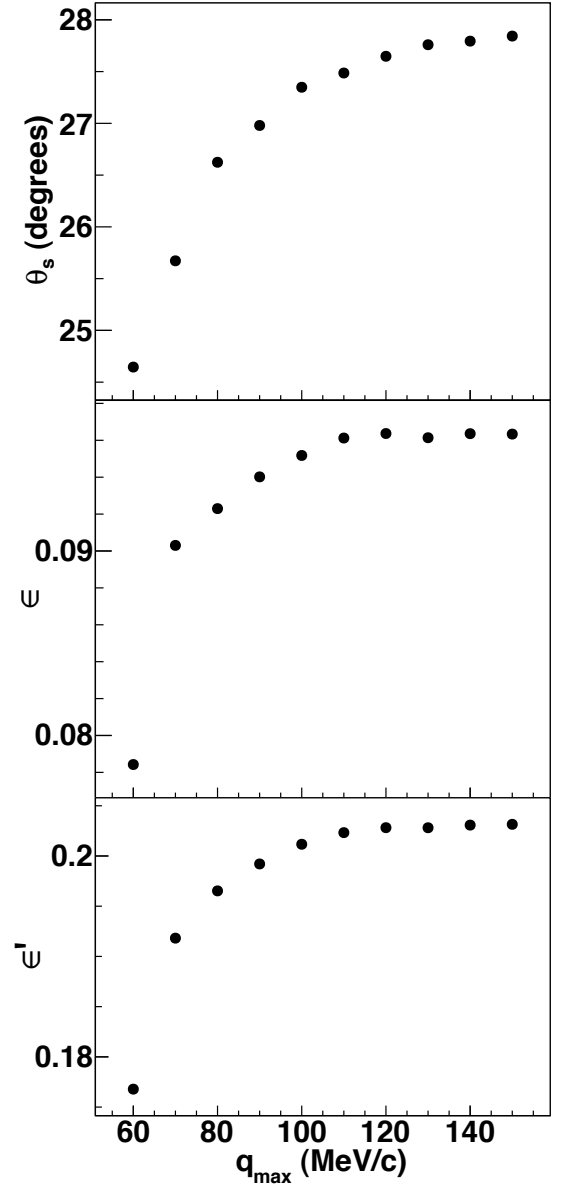

FIG. 8: Source anisotropy parameters extracted from two-pion correlation functions for UrQMD-generated Au+Au collisions at $\sqrt{s_{NN}} = 3.84$ GeV at $b = 4 - 8$ fm, are plotted as a function of the range in relative momentum over which the correlation functions are fitted. Respectively, top, middle and bottom panels show the source tilt angle θ_S, eccentricity about the beam axis ε and eccentricity about the tilted axis ε'. See text for details.

usual three), all of which depend on the pair emission angle relative to the impact parameter. The order and magnitude of the radius oscillations are quantified by Fourier coefficients, which may be directly related to the spatial tilt and eccentricity of a Gaussian source with no space-momentum correlations (arising, for example, from collective flow). For a more realistic freezeout distribution, the connection between the oscillating radii and the source anisotropy is only approximate. Using a sophisticated transport model to simulate the entire collision evolution and particle decoupling, we have studied

the freezeout distribution in coordinate space. The "whole" distribution indeed features a tilted structure and eccentricity, but shows other, less trivial anisotropic structures as well.

The experimentalist, of course, cannot study the distribution directly in coordinate space. We have simulated the experimental situation by constructing two-pion correlation functions for different pair emission angles, fitted each with a Gaussian functional form and extracted Fourier coefficients for each radius. These coefficients were then used in the formalism derived in section II to estimate the tilt and eccentricity. The agreement between these estimates of the anisotropy and the more direct study in coordinate space, was fair. Previous studies [21] of boost-invariant hydrodynamic and blast-wave models found that the eccentricity values estimated from two-particle radii were within 30% of the "true" values; this has been used as a systematic error for the eccentricity in experimental studies [10]. Our results using UrQMD are consistent with this 30% value. The present study is the first estimate of the corresponding uncertainty in the tilt, θ_S; the agreement is somewhat worse, on the order of 35%. Given the complications of dynamically-induced homogeneity regions, a time-evolving emission distribution, non-Gaussianness and "twist" effects, one might easily have expected much worse agreement.

However approximate, quantifying the connection between the radius oscillations and the underlying geometry can be useful. Ideally, the correct model of a heavy ion collision will reproduce all experimental observations; here, this means the HBT radii and their dependence on azimuthal angle. However, when observations are reproduced and others not, con-nections to the underlying scenario are important. For example, if a model reproduces R_{long} and R_{side} but over-estimates R_{out} [e.g. 44–46], attention immediately turns to emission duration, which may be associated with the nature of the transition between confined and deconfined states, latent heat, etc [28, 29, 47].

For the azimuthal dependence of HBT radii, the tilt angle and eccentricities probe different aspects of the dynamics. At AGS energies (~ 3.5 GeV), θ_S reflects the dynamics behind directed flow [20] in the earliest stage of the collision and shows strong dependence of the equation of state used in transport calculations [9]. Meanwhile, the eccentricities represent the geometric and temporal [48] aspects of elliptic flow. It is hoped that the connections we have discussed here, between experimental observations and the underlying source anisotropy, will help future comparative studies focus on the physics most relevant to each observable.

[1] Michael Annan Lisa, Scott Pratt, Ron Soltz, and Urs Wiedemann. *Ann. Rev. Nucl. Part. Sci.* 55:357–402, 2005

[2] Peter F. Kolb, Josef Sollfrank, and Ulrich W. Heinz. *Phys. Rev.* C62:054909, 2000

[3] Sergei A. Voloshin, Arthur M. Poskanzer, and Raimond Snellings. *0809.2949*

[4] M.A. Lisa et al. *Phys.Rev.Lett.* 75:2662–2665, 1995

[5] Huichao Song, Steffen A. Bass, Ulrich W. Heinz, Tetsufumi Hirano, and Chun Shen. *1011.2783*. * Temporary entry *

[6] B. A. Cole et al. *Eur. Phys. J.* C43:271–280, 2005

[7] A. Majumder. *Phys.Rev.* C75:021901, 2007

[8] Steffen A. Bass, Charles Gale, Abhijit Majumder, Chiho Nonaka, Guang-You Qin, et al. *Phys.Rev.* C79:024901, 2009

[9] M. A. Lisa et al. *Phys. Lett.* B496:1–8, 2000

[10] John Adams et al. *Phys. Rev. Lett.* 93:012301, 2004

[11] D. Adamova et al. *Phys. Rev.* C78:064901, 2008

[12] M.M. Aggarwal et al. *1007.2613*

[13] David A. Brown and Pawel Danielewicz. *Phys. Lett.* B398:252–258, 1997

[14] Sergei Y. Panitkin and David A. Brown. *Phys. Rev.* C61:021901, 2000

[15] D. A. Brown, R. Soltz, J. Newby, and A. Kisiel. *Phys. Rev.* C76:044906, 2007

[16] D. Hardtke and S. A. Voloshin. *Phys. Rev.* C61:024905, 2000

[17] Zi-wei Lin, C. M. Ko, and Subrata Pal. *Phys. Rev. Lett.* 89:152301, 2002

[18] Evan Frodermann, Ulrich Heinz, and Michael Annan Lisa. *Phys. Rev.* C73:044908, 2006

[19] A. N. Makhlin and Yu. M. Sinyukov. *Z. Phys.* C39:69, 1988

[20] Michael Annan Lisa, Ulrich W. Heinz, and Urs Achim Wiedemann. *Phys. Lett.* B489:287–292, 2000

[21] Fabrice Retiere and Michael Annan Lisa. *Phys. Rev.* C70:044907, 2004

[22] B. Tomasik. *Acta Phys. Polon.* B36:2087-2104 (2005).

[23] Ulrich W. Heinz and Peter F. Kolb. *Phys. Lett.* B542:216–222, 2002

[24] A. Kisiel, W. Broniowski, M. Chojnacki and W. Florkowski, Phys. Rev. C79, 014902 (2009)

[25] M. Csanad, B. Tomasik and T. Csorgo, Eur. Phys. J. A37, 111 (2008).

[26] A. Ster, M. Csanad, T. Csorgo, B. Lorstad and B. Tomasik, Eur. Phys. J. A47, 58 (2011).

[27] S. V. Akkelin and Yu. M. Sinyukov. *Phys. Lett.* B356:525–530, 1995

[28] S. Pratt. *Phys. Rev.* D33:1314–1327, 1986

[29] G. F. Bertsch. *Nucl. Phys.* A498:173c–180c, 1989

[30] T. Csorgo, J. Zimanyi, J. Bondorf, H. Heiselberg, and S. Pratt. *Phys. Lett.* B241:301–307, 1990

[31] Ulrich W. Heinz, A. Hummel, M. A. Lisa, and U. A. Wiedemann. *Phys. Rev.* C66:044903, 2002

[32] S. A. Bass et al. *Prog. Part. Nucl. Phys.* 41:255–369, 1998

[33] M. Bleicher et al. *J. Phys.* G25:1859–1896, 1999

[34] Hannah Petersen, Marcus Bleicher, Steffen A. Bass, and Horst Stocker. *0805.0567*

[35] Qingfeng Li, Marcus Bleicher, and Horst Stoecker. *Phys. Rev.* C73:064908, 2006

[36] Qingfeng Li, Marcus Bleicher, Xianglei Zhu, and Horst Stoecker. *J. Phys.* G33:537–548, 2007

[37] Qingfeng Li, Marcus Bleicher, and Horst Stocker. *J. Phys.* G34:2037–2044, 2007

[38] Qing-feng Li, Jan Steinheimer, Hannah Petersen, Marcus Bleicher, and Horst Stocker. *Phys. Lett.* B674:111–116, 2009

[39] S. A. Voloshin and W. E. Cleland. *Phys. Rev.* C54:3212–3217, 1996

[40] Urs Achim Wiedemann. *Phys. Rev.* C57:266–279, 1998

[41] Henning Heiselberg. *Phys. Rev. Lett.* 82:2052–2055, 1999

[42] Henning Heiselberg and Anne-Marie Levy. *Phys. Rev.* C59:2716–2727, 1999

[43] J. Adams et al. *Phys. Rev.* C71:044906, 2005

[44] Sven Soff, Steffen A. Bass, and Adrian Dumitru. *Phys. Rev. Lett.* 86:3981–3984, 2001

[45] Sven Soff, Steffen A. Bass, David H. Hardtke, and Sergey Y. Panitkin. *Nucl. Phys.* A715:801–804, 2003

[46] Ulrich W. Heinz and Peter F. Kolb. *hep-ph/0204061*

[47] Dirk H. Rischke and Miklos Gyulassy. *Nucl. Phys.* A608:479–512, 1996

[48] Michael Annan Lisa. *Acta Phys.Polon.* B35:37–46, 2004

[49] Randall Wells. *Ph.D. thesis, Ohio State University*. 2002